Contributed Papers from Materials Science and Technology 2017 (MS&T17)
October 8 – 12, 2017, David L. Lawrence Convention Center, Pittsburgh, Pennsylvania USA

DOI 10.7449/2017/MST_2017_474_481

EFFECT OF INTERCRITICAL DEFORMATION ON FINAL MICROSTRUCTURE IN LOW CARBON GRADES

U. Mayo, N. Isasti, J.M. Rodriguez-Ibabe and P. Uranga

CEIT and Tecnun (University of Navarra), San Sebastian, Basque Country, Spain

Keywords: intercritical deformation, microalloyed steels, microstructure, EBSD

Abstract

Heavy gauge line pipe and structural steel plate materials are often rolled in the two-phase region for strength reasons. However, strength and toughness show opposite trends and the exact effect of each rolling process parameter remains unclear. Even though intercritical rolling has been widely studied, further understanding of the evolution of the microstructure under intercritical conditions and the effect of different austenite-ferrite phase contents at high temperature is needed to define stable processing windows. For that purpose, laboratory thermomechanical simulations reproducing intercritical rolling conditions have been performed in low carbon steels. A methodology able to distinguish deformed ferrite from non-deformed ferrite was developed using Electron Backscattered Diffraction (EBSD) technique. The effect of chemical composition, austenite-ferrite balance and deformation on the final microstructure was evaluated. This analysis is intended to deepen the knowledge of the effect that intercritical rolling has on the microstructural evolution and, by extension, on the mechanical properties.

Introduction

Intercritical rolling is considered a promising way to optimize the final microstructure and to meet the demanding market requirements concerning mechanical properties. Intercritical rolling of steels has been studied for the last years, usually focused on the rolling load impact and specific process conditions [1-3]. Heavy gauge structural steel plates are often partially rolled in the two-phase region (austenite+ferrite) as a result of the large temperature gradients over the thickness. In these products, strength and toughness exhibit opposite trends, associated with the final microstructural heterogeneities. As strength increases due to intercritical deformation, toughness is impaired. Furthermore, the control of the final mechanical properties is more complex when compared to a standard austenitic rolling strategy, because of the combination of several microstructural phenomena, such as restoration and recrystallization taking place in both austenitic and ferritic regions. Different advanced characterization techniques, such as EBSD, have been developed in order to understand microstructure evolution when intercritical rolling is used, being able to distinguish between deformed ferrite and deformation induced transformed ferrite grains [4]. However, the exact effect of the rolling process parameters in each ferrite population is still unclear. Even though intercritical rolling has already been analyzed for plain carbon steels [3], the influence of intercritical deformation for microalloyed steels is less explored [5]. It is well known that the addition of Nb as an alloying element can retard or inhibit recrystallization of austenite and ferrite due to two mechanisms: the solute drag effect owed to Nb atoms in solid solution and the pinning effect caused by strain-induced precipitation, the latter usually exerting the strongest effect [6]. In the current work, and with the main goal of gaining a deeper understanding of the microstructure evolution during intercritical deformation, intercritical rolling simulations were carried out by dilatometry tests using a CMn and a NbV microalloyed steel. An exhaustive EBSD characterization procedure was also developed to classify and quantify the different phases.

Experimental

Chemical compositions of the studied steels are listed in Table I. In addition to a 0.06%C plain CMn steel, a NbV microalloyed steel with 0.056%Nb and 0.034%V was also selected.

Table I Chemical composition of the steels studied (weight percent).

	C	Mn	Si	P	S	Cu	V	Ti	Al	Nb	N
CMn	0.06	1.54	0.25	0.013	0.003	0.009	0.005	0.002	0.035	0.002	0.003
NbV	0.06	1.52	0.25	0.013	0.003	0.010	0.034	0.002	0.038	0.056	0.004

Uniaxial compression tests were carried out using a Bähr DIL805D deformation dilatometer. Solid cylinders of 5 mm in diameter and 10 mm in length were machined for the experiments. The CMn samples were subjected to the thermomechanical cycles depicted schematically in Figure 1a. The schedule includes an austenitization step at 900ºC during 3 minutes and afterwards, the samples were cooled down slowly (1ºC/s) to three different deformation temperatures, in order to obtain different ferrite contents before the deformation. In the NbV microalloyed steel, and after a solubilization treatment at 1250ºC for 15 minutes, two different thermomechanical schedules were defined, with the purpose of obtaining different austenite conditions (non-deformed and deformed austenite, in Cycle A and Cycle B, respectively) prior to transformation. With the aim of generating different ferrite contents of approximately 25, 50 and 75%, deformation temperatures of 760, 750 and 740ºC were selected for the CMn steel. Meanwhile, for the NbV steel, the formation of different fractions of ferrite were achieved at deformation temperatures of 740, 730 and 720ºC in Cycle A and 760, 750 and 740ºC in Cycle B (low, medium and high ferrite content, respectively). Finally, a deformation of 0.4 was applied in the intercritical region. After that, the specimens were cooled down to room temperature (1ºC/s) in both steels.

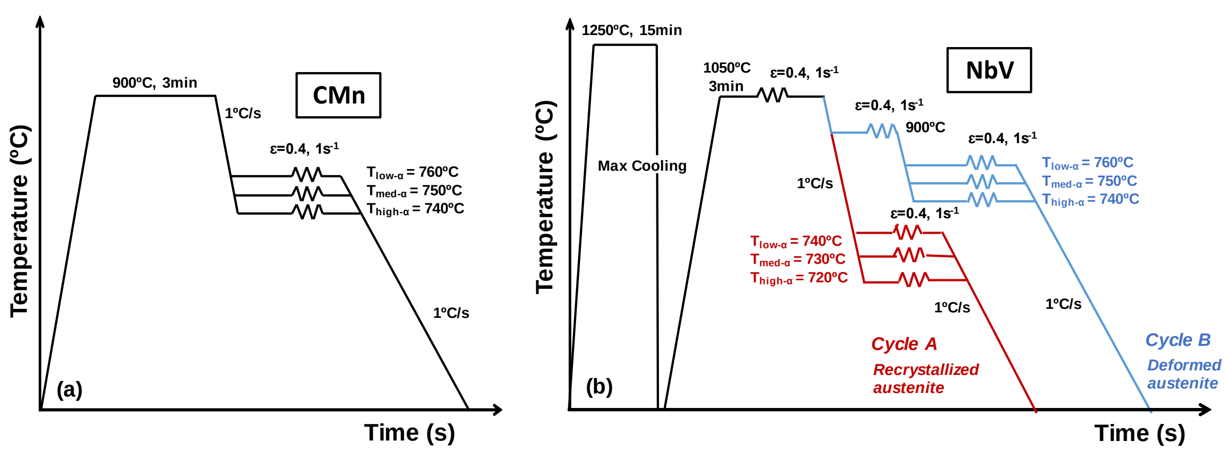

Figure 1. Thermomechanical schedule performed at the dilatometer: (a) CMn steel and (b) NbV microalloyed steel.

Results and discussion

Effect of deformation temperature in the CMn steel

The microstructures obtained in the air-cooled specimens for the CMn steel and the three deformation temperatures of 760, 750 and 740ºC are shown in Figure 2. Combinations of non-deformed and deformed ferrite are clearly distinguished in all cases. Moreover, formation of pearlite is also observed in the resulting microstructure. It is evident that the content of deformed ferrite increases as the deformation temperature is decreased, due to the higher presence of ferrite in the microstructure prior to deformation. Figure 2 shows that the deformed ferrite is characterized by a significant presence of substructure.

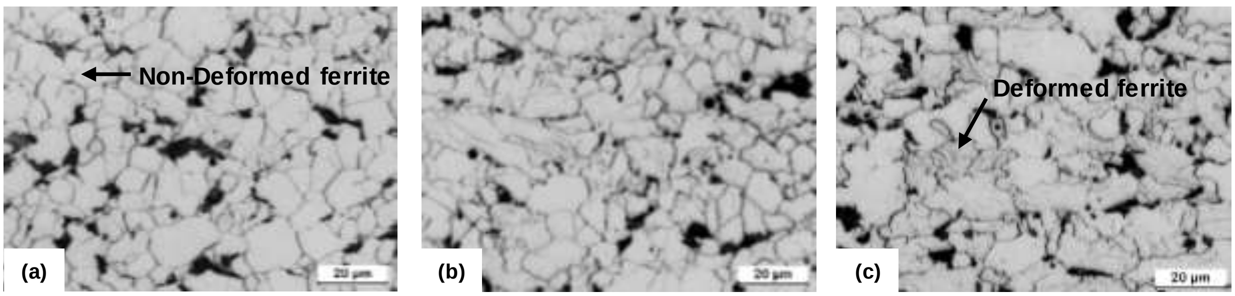

Figure 2. Optical micrographs obtained after intercritical deformation and air-cooling in the CMn steel: (a) low ferrite content (760ºC), (b) medium ferrite content (750ºC) and (c) high ferrite content (740ºC).

In the FEG-SEM micrographs shown in Figure 3 the differences between different ferrite morphologies can be appreciated more properly. Figure 3 illustrates the morphology of the phases formed at the lowest deformation temperature of 740ºC in the CMn steel. Due to the formation of a high fraction of ferrite prior to deformation, the resulting microstructure is characterized by the presence of a considerable fraction of deformed ferrite and low fraction of non-deformed ferrite, which is formed during the final air cooling step. In the deformed ferrite, a well defined substructure is clearly identified, reflecting that restoration of ferrite occurs during deformation in the intercritical region.

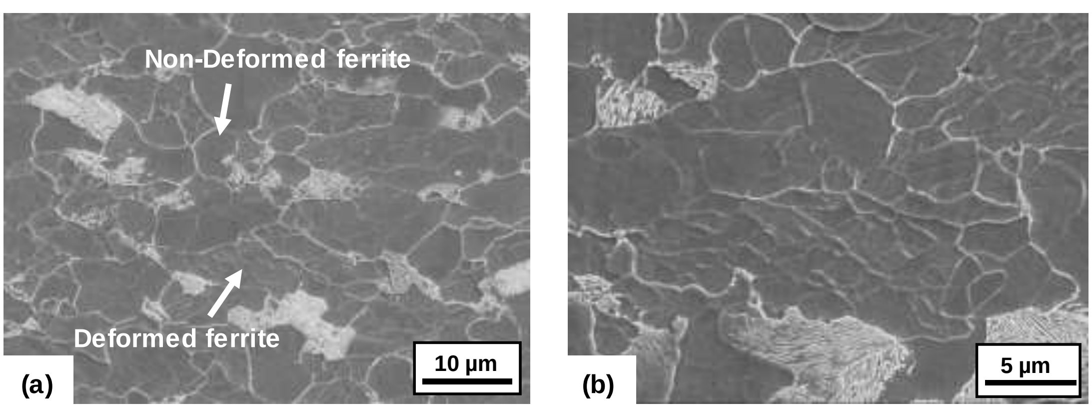

Figure 3. (a,b) FEG-SEM micrographs at different magnifications obtained after the lowest deformation temperature of 740ºC in the CMn steel.

In the current study, the microstructural analysis has been extended using the Electron Backscattered Diffraction (EBSD) technique in order to quantify the effect of the deformation temperature and the ferrite fraction before deformation. The present analysis develops a methodology for analyzing the microstructural features of a sample deformed in the intercritical region, which cannot be correctly quantified by any other standard microstructural characterization technique such as optical microscopy and/or FEG-SEM. In Figure 4, different EBSD maps corresponding to the CMn steel and deformed at 740ºC (Figure 4a Image Quality and Figure 4b Grain Boundary maps) are presented, illustrating the differences between both ferrite populations. Figure 4a clearly shows a mixture between deformed and non-deformed ferrite grains, where non-deformed ferrite grains are characterized by clearer diffraction patterns (higher IQ).

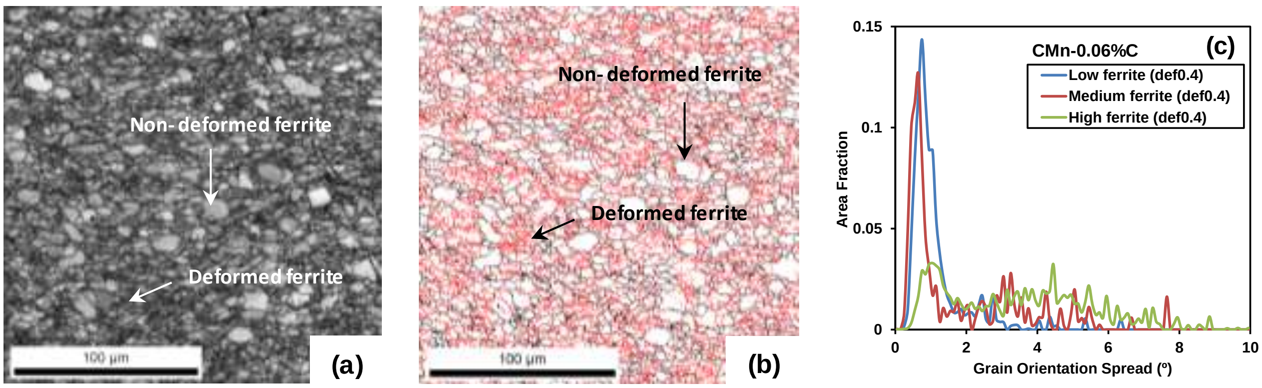

Figure 4. (a) Image Quality and (b) Grain Boundary Map (black lines for high angle misorientation criteria and red lines for low angle misorientation criteria) corresponding to the CMn steel and deformation temperature of 740ºC. (c) GOS parameter distributions for different ferrite contents (low, medium and high) in the CMn steel.

The differences between both ferrite types are also evident in the grain boundary map shown in Figure 4b. The applied deformation promotes the modification of the formed ferrite, reflected in the presence of a higher substructure (see red lines in the grain boundary map shown in Figure 4b). As mentioned previously, this could indicate the restoration of ferrite during the deformation in the intercritical region. Conversely, the ferrite grains formed during and/or after the final air cooling step don’t show any presence of low angle boundaries. Given that a combination between different ferrite populations is observed in the resulting microstructures, a methodology able to distinguish both types of ferrite was developed. First, in order to distinguish both ferrite populations, pearlite has to be deleted. A criterion based on Image Quality (IQ), which describes the quality of an electron back scattering diffraction pattern, was taken into account for the differentiation of ferrite from pearlite. Then, and for the distinction between deformed and non-deformed ferrite, the Grain Orientation Spread (GOS) parameter was considered, which is the average deviation between the orientation of each point in the grain and the average orientation of the grain. In Figure 4c GOS parameter distributions are plotted for the CMn steel and different deformation temperatures (low, medium and high ferrite contents). During the deformation, a distortion in the crystal lattice is introduced, reflected in a higher GOS parameter. Conversely, after deformation and during the slow cooling step, the formation of new ferrite grains free of deformation occurs, which are characterized by low GOS values. Therefore, as shown in Figure 4c the fraction of ferrite previous to deformation affects significantly the GOS parameter distribution. When a low fraction of ferrite is formed before deformation, a narrow GOS distribution is measured, with a considerable fraction of grains with low GOS values. This is due to the presence of high fraction of non-deformed grains (transformed after deformation) in the resulting microstructure. As ferrite content before deformation increases, GOS parameter distributions become wider and most of the grains are characterized by higher misorientation values. For each GOS distribution, a threshold GOS value was defined for the differentiation between deformed and non-deformed ferrite grains. A common value of 2º was calculated as the average of all the threshold angles defined in each scan.

Based on this GOS criterion, two ferrite populations are distinguished for each condition. Figure 5a and b, respectively, show both individual non-deformed and deformed ferrite populations with the Kernel maps superimposed. The intercritical deformation promotes the increase of the Kernel Average Misorientation value (KAM) in the deformed ferrite, reaching an average value of 1.2º in the deformed ferrite and 1º in the undeformed population (KAM measured for misorientations lower than 2º). A quantification of low and high angle misorientation unit sizes was also performed, taking into account 4º and 15º misorientation criteria (D_{4° and D_{15°). In Figure 5c mean unit sizes considering low and high misorientation criteria have been plotted for both ferrite populations (deformed and non-deformed ferrite) and different intercritical ferrite contents (low, medium and high). Regarding ferrite population corresponding to deformed grains, slightly coarser microstructures are obtained as the ferrite content prior to deformation increases, mainly for high angle unit sizes. Conversely, looking at the results related to non-deformed population, the mean grain size decreases as ferrite fraction before deformation is increased. The main difference, though, is related to the differences between D_{4° and D_{15° in the two populations. For the non-deformed ferrite, show similar D_{4° and D_{15° value, reflecting the lack of substructure. Inversely, in the deformed ferrite population, the differences between D_{4° and D_{15° are bigger due to the well-defined internal subgrain structure.

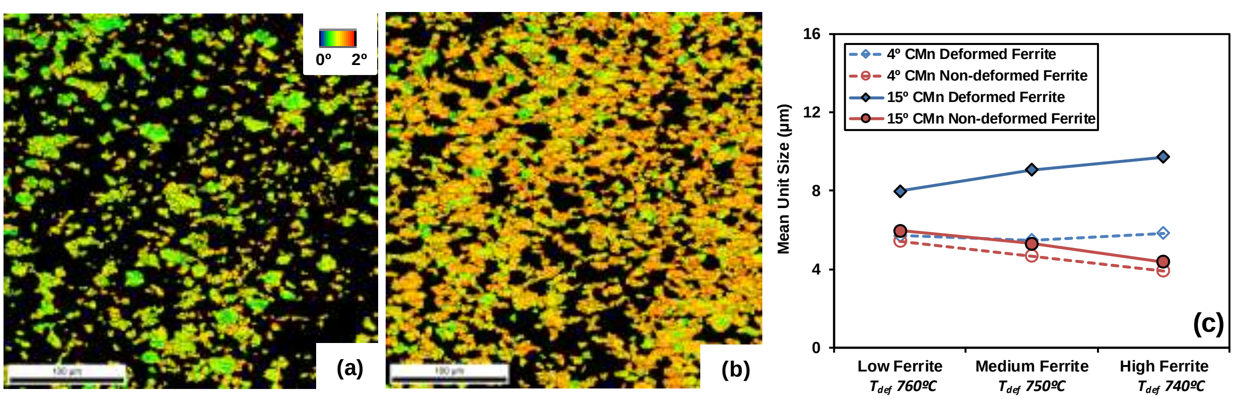

Figure 5. EBSD maps (Kernel maps) corresponding to the CMn steel and high ferrite content: (a) Non-deformed ferrite population (GOS<2º) and (b) deformed ferrite population (GOS>2º). (c) Influence of deformation temperature on mean unit sizes for both ferrite populations (low and high angle misorientation criteria).

<u>Effect of the microalloying elements in the intercritical region</u>

In order to gain a better understanding of the influence that microalloying elements have on the microstructural evolution, intercritical deformation simulations were also performed for the NbV microalloyed steel. In addition to the evaluation of the effect of different ferrite contents before deformation (see Figure 1b), the influence of the austenite conditions was also analyzed. As an example, in Figure 6, FEG-SEM micrographs corresponding to the NbV steel and the lowest deformation temperatures are presented, equivalent to a ~75% ferrite formation prior to intercritical deformation. Figure 6a corresponds to the microstructure obtained after transformation from recrystallized austenite (Cycle A) and intercritically deformed at 720ºC, whereas in Figure 6b the micrograph is relative to the sample transformed from deformed austenite (Cycle B) and a intercritical deformation temperature of 740ºC. Differences between the microstructures formed from recrystallized austenite and deformed austenite are clear. Attending to Figure 6, the addition of microalloying elements promotes the formation of more bainitic phases and reduces the presence of polygonal phases. Quasipolygonal ferrite is observed in NbV microalloyed steel and both austenite conditions. Furthermore, and when the transformation occurs from recrystallized austenite (Figure 6a), deformation bands are identified inside the deformed ferrite grains, reflecting a lack of ferrite restoration. The addition of Nb delays or suppresses the restoration of ferrite when transformation occurs from Cycle A (recrystallized austenite). Both the drag effect and/or strain induced precipitation at low temperatures (range between 740ºC and 720ºC), delay and suppress the restoration of ferrite during intercritical deformation. This behavior was already observed in previous studies [5]. However, and as previously observed in the CMn steel, presence of substructure can be appreciated in the sample transformed from deformed austenite (Figure 6b) and some subgrain formation can be seen, associated with the activation of restoration during the deformation pass. The deformation of austenite below the non-recrystallization temperature (T_{nr}) promotes strain induced precipitates at higher temperatures, which are effective pancaking austenite but they reduce the Nb available during and after transformation to interact with ferrite restoration or recrystallization phenomena.

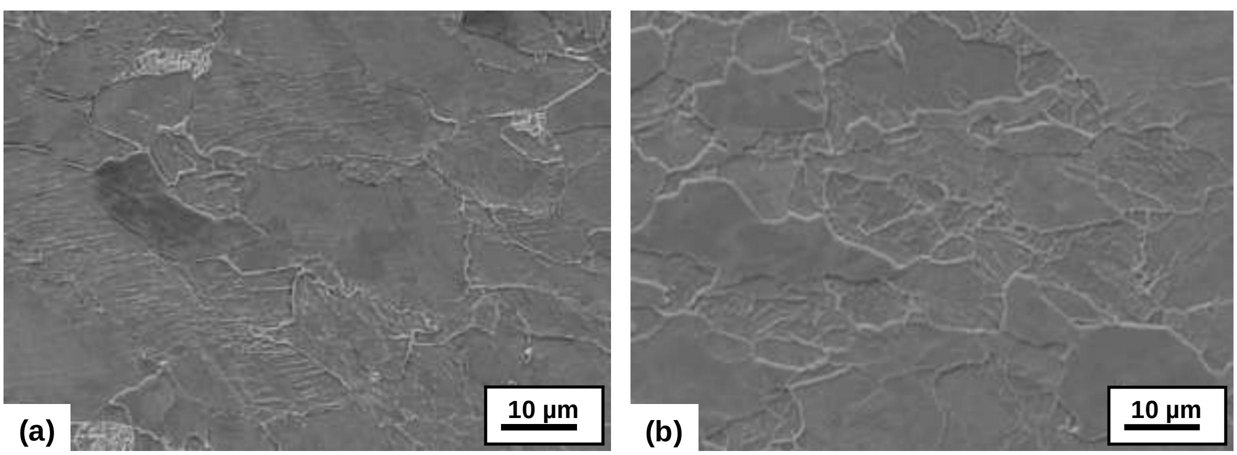

Figure 6. FEG-SEM micrographs from the NbV and the lowest deformation temperature: (a) Cycle A (transformation from recrystallized austenite) and intercritical deformation temperature of 720ºC and (b) Cycle B (transformation from deformed austenite) and deformation temperature of 740ºC.

Additionally, crystallographic characterization was performed by means of EBSD in both austenitic conditions and entire range of deformation temperatures for the NbV microalloyed steel. Given that more bainitic phases are formed when microalloying elements are added, the methodology previously shown has to be redesigned. Under both cycles (recrystallized and deformed austenite), three different populations are identified: polygonal ferrite (PF), quasipolygonal ferrite (QF) and deformed ferrite. In this case, the ferrite population with GOS values lower than 3º is considered as non-deformed ferrite, where PF and QF are included. GOS values higher than 3º correspond to deformed ferrite grains. As an example, several EBSD maps are shown in Figure 7, with a high ferrite (~75%) content prior to intercritical deformation. In Figure 7 both non-deformed (polygonal and quasipolygonal ferrite) and deformed ferrite families were split for each austenite condition. Figure 7a and c correspond to microstructures transformed from recrystallized austenite (Cycle A), whereas Figure 7b and d are related to transformation from deformed austenite (Cycle B). In these maps Inverse Pole Figures and Image Quality maps are superimposed, as well as high and low angle boundaries (coarse and fine black lines, respectively). Concerning non-deformed ferrite populations, finer microstructures are formed when the transformation occurs from recrystallized austenite (see Figure 7a). The mean unit size considering low angle boundaries decreases from 3.9 to 3.5 µm, for deformed austenite and recrystallized austenite, respectively. Higher transformation start temperatures are measured in the samples corresponding to Cycle B (deformed austenite), leading to the formation of slightly coarser microstructures.

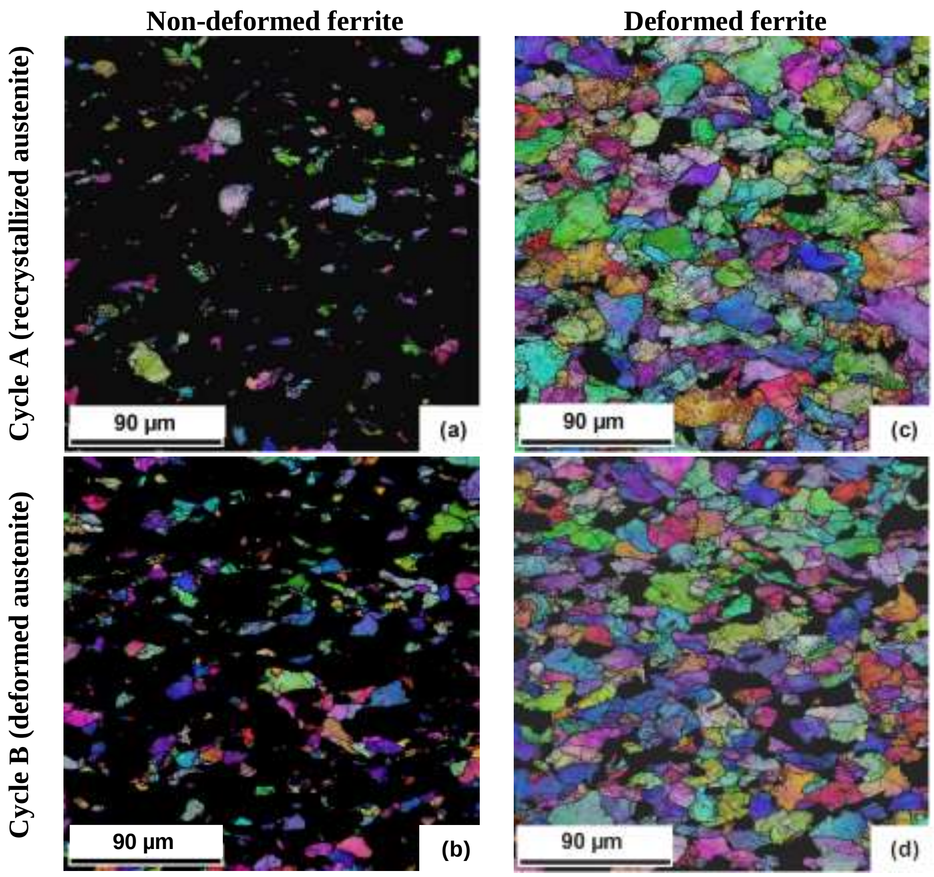

Figure 7. Inverse Pole Figure and Image Quality maps superimposed, as well as high and low angle boundaries (coarse and fine black lines) for NbV steel, high ferrite content and both populations (non-deformed and deformed ferrite): (a,c) recrystallized austenite (Cycle A) and (b,d) deformed austenite (Cycle B).

Conversely, a microstructural refinement in the deformed ferrite is clearly observed when the transformation takes place from a deformed austenite (Cycle B in Figure 7d). Taking into account high angle boundaries, mean grain size of 15.1 and 12.9 µm are measured, for Cycles A and B, respectively. The ferrite refinement caused by deformed austenite is related to the increase of the specific grain boundary area and is attributed to a significant increase in the density of ferrite nucleation sites [7]. Moreover, the low angle boundaries drawn in the IPF maps indicate that a completely different substructure is formed inside the deformed ferrite grains for each austenite condition (see Figure 7c and d). In the microstructure corresponding to Cycle A deformation bands can be clearly distinguished (parallel microbands), attributed to the potential of Nb delaying ferrite restoration (see Figure 7c). Conversely, the presence of sub-boundaries (low angle boundaries represented in fine black lines) is confirmed when the austenite is deformed in the non-recrystallization region (see Figure 7d).

Conclusions

An exhaustive EBSD characterization procedure is proposed to determine and quantify the different ferrite phases formed after intercritical deformation. The threshold values to differentiate between deformed and non-deformed ferrite are different in CMn and NbV microalloyed steels. This is due to the different nature of the ferrite and the variation of internal substructure and dislocation densities in each material. The transformation of ferrite from recrystallized and deformed austenite infers modifications in the intercritically deformed ferrite. Differences in the niobium available during transformation are a key factor to maintain the deformation bands or to develop a substructure within the intercritically deformed grains.

Acknowledgements

The financial support of the Spanish Ministry of Economy and Competitiveness (MAT2015-69752) is gratefully acknowledged. The authors also acknowledge a research grant from the European Commission Research Fund for Coal and Steel (RFSR-CT-2015-00014).

References

[1] S. Gohda, K. Watanabe, Y. Hashimoto, “Effects of the intercritical rolling on structure and properties of low carbon steel”, *Transactions ISIJ*, 21 (1981), 6-15.

[2] M. R. Barnett and J. J. Jonas, “Distinctive Aspects of the Physical Metallurgy of Warm Rolling.,” *ISIJ Int.*, 39 (1999), 856–873.

[3] A. O. Humphreys, D. Liu, M. R. Toroghinejad, E. Essadiqi, and J. J. Jonas, “Warm rolling behaviour of low carbon steels”, *Mater. Sci. Technol.*, 19 (2003), 709–714.

[4] B. Eghbali, “Microstructural development in a low carbon Ti microalloyed steel during deformation within the ferrite region”, *Mat. Sci. Eng. A*, 480A (2008), 84–88.

[5] E.A. Simielli, S. Yue, and J.J. Jonas, “Recrystallization Kinetics of Microalloyed Steels Deformed in the intercritical Region”, *Met. Trans. A*, 23A (1992), 597-608.

[6] O. Kwon and A.J. DeArdo, “Interactions between Recrystallization and Precipitation in Hot-Deformed Microalloyed Steels”, *Acta Mater.*, 39 (1991), 529-538.

[7] N. Isasti, D. Jorge-Badiola, M. L. Taheri, and P. Uranga, “Phase transformation study in Nb-Mo microalloyed steels using dilatometry and EBSD quantification”, *Metall. Mater. Trans. A,* 44A (2013), 3552-3563.